

Tropical Precipitation Extremes

WILLIAM B. ROSSOW

Cooperative Remote Sensing Science and Technology Institute at The City College of New York, New York, New York

ADEME MEKONNEN

Energy and Environmental Systems Department, North Carolina A&T State University, Greensboro, North Carolina

CINDY PEARL

Cooperative Remote Sensing Science and Technology Institute at The City College of New York, New York, New York

WEBER GONCALVES

Instituto Nacional de Pesquisas Espaciais, Centro de Previsão de Tempo e Estudos Climáticos, Sao Paulo, Brazil

(Manuscript received 7 December 2011, in final form 24 August 2012)

ABSTRACT

Classifying tropical deep convective systems by the mesoscale distribution of their cloud properties and sorting matching precipitation measurements over an 11-yr period reveals that the whole distribution of instantaneous precipitation intensity and daily average accumulation rate is composed of (at least) two separate distributions representing distinctly different types of deep convection associated with different meteorological conditions (the distributions of non-deep-convective situations are also shown for completeness). The two types of deep convection produce very different precipitation intensities and occur with very different frequencies of occurrence. Several previous studies have shown that the interaction of the large-scale tropical circulation with deep convection causes switching between these two types, leading to a substantial increase of precipitation. In particular, the extreme portion of the tropical precipitation intensity distribution, above 2 mm h^{-1} , is produced by 40% of the larger, longer-lived mesoscale-organized type of convection with only about 10% of the ordinary convection occurrences producing such intensities. When average precipitation accumulation rates are considered, essentially all of the values above 2 mm h^{-1} are produced by the mesoscale systems. Yet today's atmospheric models do not represent mesoscale-organized deep convective systems that are generally larger than current-day circulation model grid cell sizes but smaller than the resolved dynamical scales and last longer than the typical physics time steps. Thus, model-based arguments for how the extreme part of the tropical precipitation distribution might change in a warming climate are suspect.

1. Introduction

Some of the concern about possible negative impacts of a warming climate is focused on possible increases of precipitation extremes. For the case of large precipitation amounts that cause flood damage, larger total accumulation can be produced by events with larger average precipitation intensities (average of the instantaneous

intensity in mm h^{-1} over space and time, excluding the zero values), events with more moderate average intensities but longer durations (and slower motions), or even more frequent events of moderate average intensity. Discussions of climate model behavior (e.g., Meehl et al. 2005) often focus on extremes of total precipitation accumulation (expressed as an average accumulation rate, either in mm h^{-1} or in mm day^{-1} , the average intensity but with zero values included), whereas observational studies, especially satellite-based ones, often focus on the precipitation intensity and its frequency of occurrence (e.g., Zipser et al. 2006; Stephens et al. 2010; Lee et al. 2013). To distinguish between these

Corresponding author address: Dr. William B. Rossow, CREST Institute at The City College of New York, Steinman Hall (T-107), 140 Street & Convent Avenue, New York, NY 10031.
E-mail: wbrossow@ccny.cuny.edu

two kinds of precipitation extremes in this paper, we will refer to the instantaneous precipitation and its average (excluding zero) values as the intensity and average intensity, respectively, and refer to the daily accumulated amount of precipitation in terms of an average precipitation accumulation rate (or just rate average intensity including zero values).

Changes of the global total precipitation in a warming climate are constrained by changes in the net surface radiation and not the total water vapor abundance, because the global total precipitation has to equal the global mean surface evaporation (cooling) that balances (approximately) the surface net radiative heating. This constraint on total precipitation means that it will increase in a warming climate more slowly than the water vapor abundance (e.g., Allen and Ingram 2002; O’Gorman and Schneider 2009; Stephens and Hu 2010). Regional changes in precipitation will not necessarily follow the global constraint. The simplest argument for an increase of extreme precipitation in a warming climate is that, since the amount of precipitation produced by extreme precipitation events far exceeds the local, within-storm-area water vapor supply from the atmospheric column and surface, such storms must be fed by larger-scale moisture convergence, which would scale like increases in the water vapor abundance, all other things being equal (e.g., Trenberth et al. 2003). Hence, if precipitation extremes were to increase like the water vapor abundance in a warming climate, but the total precipitation were to increase more slowly, the frequency of all precipitation events would have to decrease (Trenberth et al. 2003). Whether the required decrease appears uniformly over the whole precipitation intensity distribution or is limited to some portion of the distribution is not obvious and likely depends on the controlling dynamics.

Allan and Soden (2008) look at how precipitation distributions change by examining observed and modeled changes during El Niño events. They show that the frequency of lighter precipitation decreases and the frequency of the heaviest precipitation increases in one dataset [the combined Remote Sensing Systems, version 6 (RSS-V6) + Global Precipitation Climatology Project (GPCP) dataset studied by Wentz et al. (2007)]—that is, that there is a shift of the whole distribution to larger values—but also show that a variety of climate models all exhibit increases of both the lightest and heaviest precipitation frequencies (i.e., a change of the distribution shape; see also Feldl and Roe 2011). We also note in passing that the Allan and Soden (2008) study documents the fact that “extreme” precipitation in climate models is very different from what is observed: of the 10 models considered, 9 have 95th percentile precipitation rates (mm day^{-1}) that are 3 to 4 times smaller than those

observed in the combined RSS-V6 + GPCP dataset. In other words, most climate models exhibit precipitation rates that are concentrated at much too small values and, since their global total precipitation is approximately correct because of energy balance, they exhibit much too frequent precipitation events (cf. Stephens et al. 2010). In any case, current atmospheric models exhibit changes of extreme tropical precipitation rates that do not scale with water vapor changes (Allen and Ingram 2002; Held and Soden 2006; Kharin et al. 2007). Regional observation-based analyses also do not show such simple scaling (e.g., Groisman et al. 2005; Lenderink and van Meijgaard 2008). Since changes in total precipitation, particularly in the tropics, imply changes in the latent heating of the atmosphere and the consequent strength of the whole general circulation, this dynamic feedback might explain why the changes in the extreme part of the precipitation distribution are different from changes of the average precipitation (Emori and Brown 2005; Held and Soden 2006). But exactly which modeled changes appear, especially in the extreme part of the distribution, is strongly dependent on the particular convection parameterization employed (cf. Zhang and McFarlane 1995; Jakob and Siebesma 2003; Hourdin et al. 2006; Kharin et al. 2007; Jung et al. 2010). This parameterization dependence may explain why the model agreement for precipitation changes with changing climate is much poorer in the tropics than in the extratropics (Kharin et al. 2007; O’Gorman and Schneider 2009). In at least one model, precipitation changes with climate are smaller than the effects of changing the convective parameterization (Wilcox and Donner 2007).

In almost all of the discussion in the literature on the topic of extreme tropical precipitation, tropical deep convection is considered to be a single phenomenon producing a continuum of precipitation intensities. For instance, the model-based study of Emori and Brown (2005) and the discussion in Held and Soden (2006) both assume that tropical deep convection is a single phenomenon. Theoretical analyses often take this approach as well; for example, Katz (1999) concludes in a case study that the most important change of precipitation distribution is not the distribution shape factor but the scale factor determining the frequency of occurrence as if the changes are distributed across the whole accumulation amount distribution.

Recent observational analyses of tropical cloud properties and behavior based on the International Satellite Cloud Climatology Project (ISCCP) products (Rossow and Schiffer 1999) have drawn attention to the fact that there is more than one type of tropical deep convection (Jakob and Tselioudis 2003; Jakob et al. 2005; Rossow et al. 2005a; Jakob and Schumacher 2008; Tromeur and

Rossow 2010; Tselioudis and Rossow 2011; Mekonnen and Rossow 2011; Lee et al. 2013), but this recognition is not really new as attested to in comprehensive reviews of earlier conventional observations of tropical storm systems (e.g., Houze and Hobbs 1982; Cotton and Anthes 1989; Emanuel 1994; Houze 2004). Satellite-based size and lifetime distributions have also suggested a range of deep convection types and that deep convective system size and duration increase together (e.g., Machado et al. 1998). Theoretical studies have long examined a number of reasons for these different types of tropical convective systems (Moncrieff 1981, 1992, 2004; Houze 2004). Tromeur and Rossow (2010) specifically show that the weather states, defined by distinctive mesoscale patterns of cloud property joint distributions in the ISCCP products (see section 2b), have very different average precipitation intensities associated with them (cf. Mohr et al. 1999; Houze 2004; Lee et al. 2013).

Many previous studies have recognized the occurrence of different types of deep convective cloud systems in the tropics, but the study of the Madden–Julian oscillation (MJO) by Tromeur and Rossow (2010) and the initiation of African easterly waves by Mekonnen and Rossow (2011) shows that both of these phenomena involve a distinct “switching” of deep convection types in the interaction with the large-scale circulation that is also associated with a characteristic increase in precipitation. In other words, the large-scale wave disturbances change the predominant type of deep convection, switching from a type with a much smaller precipitation rate to a type with a much larger precipitation rate, suggesting a positive feedback on the large-scale waves. This switching also suggests that scattered, smaller-scale, ordinary deep convection cannot “obtain” enough water vapor to produce the much larger precipitation intensities of the mesoscale systems and implies that mesoscale organization on a larger scale is required to produce truly extreme precipitation events. This behavior also raises the possibility that such dynamic switching could play a role in how extreme precipitation changes with climate.

Mohr et al. (1999) used one year of 85-GHz brightness temperatures from the Special Sensor Microwave Imager (SSM/I) to classify tropical objects by size (two categories divided by a system area equivalent to a radius of about 25 km) and convective intensity and used the same data to estimate precipitation intensity as well. They concluded that more than 70% of the total tropical precipitation is produced by the larger systems that represent fewer than 20% of precipitating systems. Note that the microwave measurements are only sensitive to the precipitating portion of these cloud systems, not the whole cloud system, so the sizes mentioned above are

smaller than the whole-system sizes discussed later. We note that Houze (2004) also states that the mesoscale convective systems account for most of the tropical precipitation.

Here, we exploit more than a decade of independent cloud and precipitation data products covering the whole tropics (15°S–15°N) to more clearly separate the contributions to average precipitation intensity and daily average accumulation rate made by the different types of deep convective systems.

2. Datasets

a. Precipitation

TRMM MULTISATELLITE PRECIPITATION ANALYSIS

The main precipitation dataset we use for this analysis is the Tropical Rainfall Measuring Mission (TRMM) Multisatellite Precipitation Analysis TRMM 3B42, version 6 (TMPA; Kummerow et al. 2000; Huffman et al. 2007), to examine the effects of different space and time resolutions on the distribution of precipitation intensity and rate. TMPA combines various products into a $0.25^\circ \times 0.25^\circ$ horizontal grid covering 50°S–50°N, including satellite passive microwave precipitation estimates from SSM/I, the Advanced Microwave Scanning Radiometer for Earth Observing System (AMSR-E), and the Advanced Microwave Sounding Unit (AMSU); satellite infrared (IR) estimates; and precipitation gauge measurements (over land). We use the period 1998–2008. TMPA is similar to the Global Precipitation Climatology Project [we compare precipitation rates with the GPCP product One-Degree Daily (1DD), version 1.1; Huffman et al. 2001; Adler et al. 2003] in its use of land-based gauge data to adjust the satellite retrievals at the monthly level, but it uses a different passive microwave algorithm and more microwave satellites. The TMPA algorithm is trained by the TRMM combined precipitation radar and passive microwave product (2B31; Kummerow et al. 2000). We interpret the quantity that is reported in TMPA at 3-h intervals to be an estimate of precipitation intensity. However, we note that extreme values of precipitation intensity in the TMPA dataset are about 10–15 mm h⁻¹, whereas the extreme values shown by Berg et al. (2010) from the TRMM Precipitation Radar approach 100 mm h⁻¹.

b. Tropical deep convection types

1) ISCCP WEATHER STATE PRODUCT

One of the ISCCP products (called D1) reports the satellite-derived properties of clouds for a 2.5° horizontal map grid over the globe at 3-hourly intervals from

July 1983 through December 2009, including joint mesoscale distributions of cloud-top pressure and optical thickness during daytime (Rossow and Schiffer 1999). A statistical analysis of these joint frequency histograms has identified distinct patterns, called weather states (WS), that have been shown to be associated with different atmospheric conditions (Jakob and Tselioudis 2003; Jakob et al. 2005; Jakob and Schumacher 2008). The ISCCP WS products are produced by analyzing the whole data record to identify the WS patterns and then classifying each individual D1 joint histogram by which of the WS it most closely resembles [see details of the method in Rossow et al. (2005a)]. To date, this analysis has been performed for four different latitude zones: the tropics ($\pm 15^\circ$ latitude), the extended tropics ($\pm 35^\circ$ latitude), and the northern and southern midlatitudes (30° – 65° latitude in each hemisphere), covering the period from July 1983 through December 2009. These data products are available from <http://crest.ccnycunyu.edu/rscg/products.html>. In the tropics (Rossow et al. 2005a), the WS have been shown to be associated with very different average precipitation rates (Tromeur and Rossow 2010; Lee et al. 2013) and radiative effects (Oreopoulos and Rossow 2011), and to exhibit different behavior in interactions between deep convection and large-scale waves (Tromeur and Rossow 2010; Mekonnen and Rossow 2011).

In this study we use the tropics' WS product: the six WS patterns of cloud-top pressure and optical thickness are shown in Fig. 1 (Rossow et al. 2005a). To understand these WS, first notice that the frequency (indicated by color in the figure) of each pair of cloud properties is related to the average fraction of the area covered by clouds with those properties: the larger the frequency, the larger the fraction of the 2.5° map grid cell covered. Second, remember that a number of studies have shown that thicker (optical thicknesses >23), higher-topped (top pressures <440 mb) clouds in the upper right in these histograms are closely related to deep convective towers, higher-topped but moderately thick clouds are related to mesoscale anvil clouds, and higher-topped but optically thin clouds are cirrus [see a summary of these results in Rossow and Schiffer (1999)]. Thus, these six WS are described as follows.

WS1 is dominated by mesoscale anvil clouds but also includes the largest area covered by deep convective clouds of any WS. WS2 is also composed of mesoscale anvil clouds with very few deep convective clouds. We know that these anvil clouds are mesoscale because the average cloud cover for these two WS is >0.9 (see next section). WS3 is dominated by less thick (<10) and lower-topped clouds that are mixed with a small fraction of deep convective clouds, more than in WS2, as well as

some cumulus congestus (very optically thick but mid-level cloud tops). Note that only clouds with optical thicknesses greater than about 20 produce any appreciable precipitation (Lin and Rossow 1997). Note also that about one-third of the dominant cloud type in WS3 (midlevel, low to moderate optical thickness) is known to be composed of thin cirrus overlying boundary layer clouds, which ISCCP places at middle levels (cf. Jin and Rossow 1997; Rossow et al. 2005b; Rossow and Zhang 2010). Finally, note that a recent analysis of *CloudSat* cloud profiles indicates that about half of what are called cumulus congestus are actually just transient deep convective clouds still growing upward (Luo et al. 2009). The key fact about WS3 is that it contains deep convective clouds but their small frequency of occurrence (coverage) indicates their small size, equivalent to isolated cumulonimbus.

For completeness, we also describe the three "non-convective" WS. WS4 is dominated by cirrus (optically thin, high topped) clouds with small amounts of cumulus (small optical thickness, low topped) clouds as well as some clouds at all levels, which are, in part, mixtures of cirrus and boundary layer clouds (Rossow et al. 2005b). WS5 is dominated by low-topped clouds with relatively smaller optical thicknesses, interpreted to be shallow cumulus, and WS6 has thicker low-topped clouds characteristic of stratocumulus and stratus clouds.

The major distinction among these WS is that the first three contain or are closely associated with deep convection and the last three states represent suppressed conditions with only shallow (boundary layer) convection (Jakob and Tselioudis 2003; Jakob et al. 2005; Rossow et al. 2005a). The key point for this paper is that this analysis shows that there are (at least) two different types of deep convective WS in the tropics, identified as WS1 and WS3. All of the studies with the tropical WS have shown a very close association of WS1 and WS2 (henceforth WS12), where WS1 is the core and WS2 is the mesoscale anvil of the convective systems that are much larger than the 2.5° grid cell. These systems have the largest areas (indicated by large frequencies in Fig. 1) covered by deep convective clouds (cf. Oreopoulos and Rossow 2011). On the other hand, WS3 contains only a small area covered by deep convective clouds, interpreted to be ordinary deep convection.

2) ISCCP CONVECTIVE SIZE/CONVECTIVE TRACKING PRODUCTS

To further distinguish the differences of deep convective types, we use the WS to composite another ISCCP-based product obtained from the analysis procedure of Machado et al. (1998). This analysis identifies contiguous regions using infrared brightness temperatures

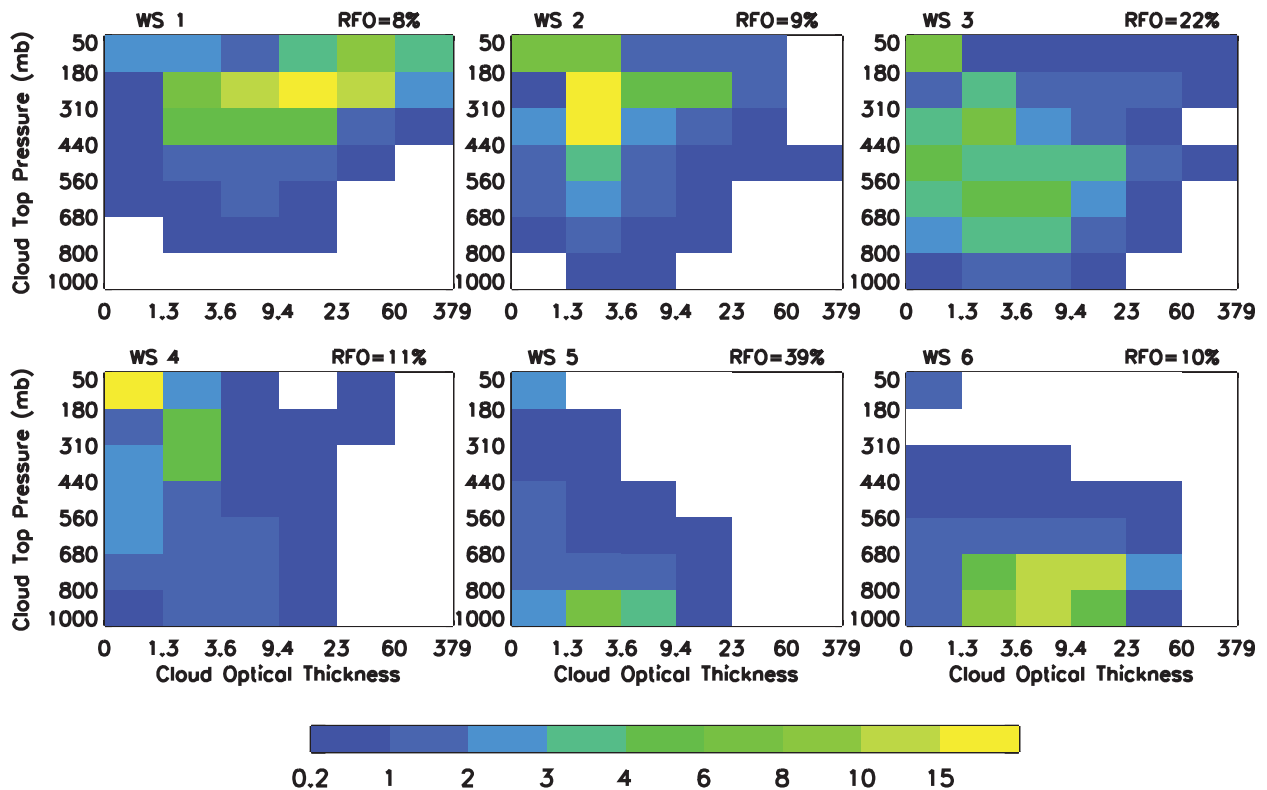


FIG. 1. Six distinctive patterns, called weather states (WS), found in the joint mesoscale frequency distributions of cloud-top pressure (mb; vertical axis) and optical thickness (unitless; horizontal axis) obtained from the analysis of individual daytime histograms of these cloud properties in the ISCCP D1 data product from July 1983 through June 2008 in the tropical zone ($\pm 15^\circ$). The colors indicate the frequency of each pair of cloud-top pressures and optical thicknesses values as area cloud fractions (in percent; these values do not add to 100% because clear sky is excluded). The relative frequency of occurrence (RFO) for each WS is shown.

(T_b) of cold cloud tops ($T_b < 245$ K) and convective cloud tops ($T_b < 220$ K) in each geostationary satellite image at 3-h intervals and tracks the motion and evolution of the larger systems [see Machado and Rossow (1993) and Machado et al. (1998) for a discussion of these thresholds]. The first analysis step produces the ISCCP convective size (CS) product, which contains information about the sizes and properties of all cold cloud objects. The second analysis step produces the ISCCP convective tracking (CT) product (available online at <http://isccp.giss.nasa.gov>) with additional information about the time variation of the cold cloud objects, including their motion, sizes, and durations. Both of these products currently cover the period from July 1983 through June 2008. The ISCCP CS dataset is here used to determine the WS sizes only for cold cloud systems containing deep convective clouds, where size is expressed as the radius of a circle with the same area down to a limit of 17 km (the area of the convective system cloud is larger than the precipitating cloud area and the updraft area; Machado et al. 1998). The WS1 size distribution peaks at about 124 km, whereas the size distribution of

WS3 systems peaks at the smallest size that can be estimated by the CS dataset (17 km). The CT dataset is used to determine the durations of the different types of deep convection: most WS3 systems have durations < 6 h, the lower limit for tracking systems in the CT dataset, whereas most WS1 systems have durations > 6 h.

3. Precipitation intensity/rate distributions and extreme values

The shape of the precipitation intensity distribution is sensitive to how the frequency histogram is formed as demonstrated by the wide variety of approaches reported in the literature. We choose to display, as a function of intensity (or rate), the frequency of occurrence multiplied by the intensity (or rate) and divided by the total precipitation amount so that the vertical axis shows the fractional contribution in percent of each intensity (or rate) range bin to the total rainfall. Different bin widths also affect the distribution shape; we choose equal intervals of 0.15 mm h^{-1} (or mm day^{-1}) to better capture the contribution of the smaller intensities (or rates), but

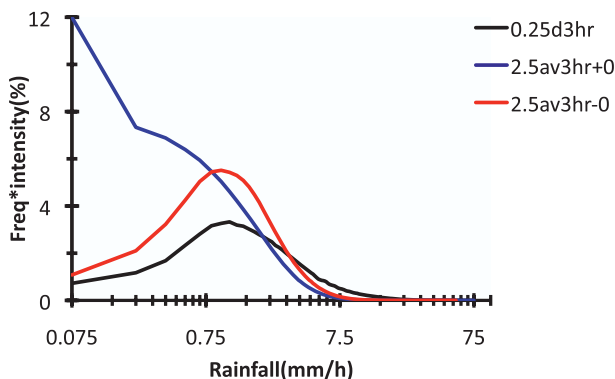


FIG. 2. Distribution of precipitation intensities (mm h^{-1}) from TMPA at 3-h intervals at 0.25° and averaged to a 2.5° resolution with (+0) and without (-0) zero values included. The vertical axis shows the frequency of occurrence of each value, binned uniformly at 0.15 mm h^{-1} intervals, multiplied by the intensity to represent the fractional contribution in percent of each intensity range to the total precipitation. The intensities are displayed on a logarithmic scale (which distorts areas) to show the contribution of the largest intensities more clearly.

plot the results against the log of intensity (or rate) to more clearly show the larger values. This choice distorts the areas in the plot so that the figures cannot be used to judge the total contribution of each range of precipitation intensity/rate. Instead we provide tables that give the distribution percentiles. To define the extreme, we follow the recommendation in Nicholls and Murray (1999) to quantify some large percentile (e.g., 95th) of the distribution of daily average precipitation rate, but focus on a similar metric for precipitation intensity. Note that we give percentile values for the precipitation intensity (or rate) distributions in the tables but we plot the fractional contribution of each intensity (or rate) in the figures. Thus, when we mention percentile values in the text and tables, it refers to the percent of the total population of events, not to the percent of the total precipitation. Remember that we refer to precipitation intensity in millimeter per hour as the instantaneous or average precipitation intensity, excluding zero values, and the average precipitation rate, which includes zero values in the average and is reported in either millimeter per hour or millimeter per day.

For this analysis, we treat the original resolution TMPA values at 0.25° and 3-h intervals as representing the instantaneous precipitation intensity distribution, but note that the higher-resolution TRMM Precipitation Radar (PR) data [about 5 km compared to 25 km; shown, e.g., in Berg et al. (2010)] has extreme values almost 5 times larger than TMPA. Figure 2 further illustrates the effect on the precipitation intensity distribution from TMPA produced by averaging the 0.25° data over a larger spatial domain to match the ISCCP WS resolution (2.5°).

TABLE 1. Percentile values of the tropical precipitation intensity (mm h^{-1}) distribution from TMPA at different spatial resolutions (0.25° , 1.0° , and 2.5°) with (+0) and without (-0) zero values included.

Percentiles	0.25°	1° avg -0	2.5° avg -0	1° avg +0	2.5° avg +0
10	0.08	0.074	0.085	0.009	0.003
20	0.23	0.193	0.221	0.031	0.01
30	0.43	0.345	0.38	0.063	0.023
40	0.66	0.515	0.552	0.114	0.046
50	0.90	0.702	0.738	0.197	0.086
60	1.20	0.923	0.958	0.331	0.154
70	1.61	1.216	1.243	0.554	0.273
80	2.29	1.65	1.646	0.954	0.495
90	3.61	2.509	2.37	1.816	0.994
95	5.25	3.549	3.165	2.842	1.599
99	11.50	6.731	5.312	5.921	3.268

As expected, the spatially averaged intensity (zero values excluded) decreases, especially the extreme (95th percentile) values, which decrease by almost a factor of 2, producing more frequent intensities at and below 1 mm h^{-1} (Table 1). Nevertheless, the smaller shift of the intensity distribution near $1\text{--}2 \text{ mm h}^{-1}$ produced by spatial averaging suggests that the spatial scale of larger intensity events is larger than 25 km (see section 4). Also shown in Fig. 2 and Table 1 is the effect of including zero values in the spatial average; the most significant change is that more than 70% of the precipitation distribution is at intensities $<0.2\text{--}0.3 \text{ mm h}^{-1}$ instead of only 25% originally. Extreme precipitation intensity decreases by almost another factor of 2.

Figure 3 illustrates the effect on the precipitation intensity distribution produced by averaging over one day at 0.25° resolution. Again we see the expected shift to smaller intensities, especially when zero values are included, but the decrease of the extreme values is only about 30%, which can be understood by the fact that the convective systems producing the extreme intensities and rates are longer lived than 3 h (see section 4). Table 2 shows the daily-averaged precipitation accumulation rates at 1.0° from TMPA: notably, the daily average rates in the large extreme part of the distribution are not that much smaller than the daily average intensities. Table 2 also compares the daily average TMPA distributions with the GPCP-1DD distribution. This comparison suggests that the GPCP dataset is more like the average precipitation intensity from TMPA than the average accumulation rate, but with much larger extreme values, which might cause some confusion.

4. Results and discussion

Figure 4 shows the precipitation intensity distributions of the ISCCP WS matched at 2.5° and 3-h intervals

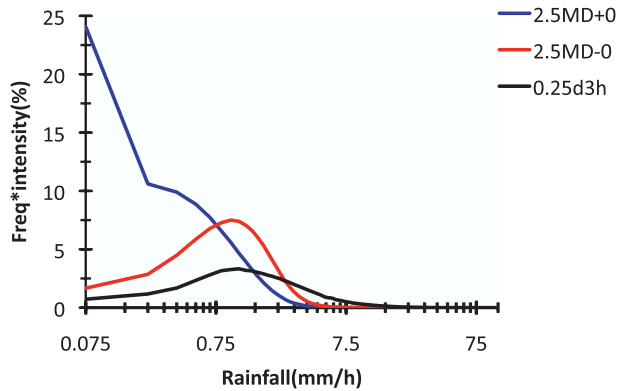


FIG. 3. Distribution of precipitation intensities (mm h^{-1}) from the original TMPA (3 h, 0.25°) and the daily average distributions with (+0) and without (-0) zero values included. The vertical axis shows the frequency of occurrence of each value, binned uniformly at 0.15 mm h^{-1} intervals and multiplied by the intensity to represent the fractional contribution in percent of each intensity range to the total precipitation. The intensities are displayed on a logarithmic scale (which distorts areas) to show the contribution of the largest intensities more clearly.

to the TMPA data for 1998–2008. WS12 clearly dominates the large extreme portion of the tropical precipitation intensity distribution with a peak contribution at about 2 mm h^{-1} that is nearly double the intensity at the peak for WS3. WS2 actually exhibits an intensity distribution similar to that for WS3 (not shown). For completeness, we also show in Fig. 4 the combined precipitation intensity distribution for the three suppressed weather states, WS4 through WS6, called WS4–6. Although these states are the “non-deep-convective” states that are mixtures of cirrus, some optically thin middle-level clouds, and shallow boundary layer convection that dominate the light precipitation part of the distribution, there are still occasional heavier ($>1 \text{ mm h}^{-1}$) precipitation events mixed in (remember that the weather state classification is a statistical resemblance classification). In fact, Lee et al. (2013) show that all of the WS exhibit larger precipitation intensities if they are preceded or followed by WS1 within 3–6 h. In other words, the heavier events in the WS4–6 distribution are closely associated with WS1 events.

Our key result is that WS12 totally dominates the precipitation intensity distribution (Fig. 4) at values $>2 \text{ mm h}^{-1}$, whereas smaller-scale, ordinary deep convection is only an important contribution (comparable to WS4–6) at values $<2 \text{ mm h}^{-1}$. In other words, the large extreme part of the precipitation intensity distribution is associated with a completely different type of deep convection than the type of deep convection that contributes to the middle range of the intensity distribution. Table 3 emphasizes this conclusion by showing

TABLE 2. Percentile values of the daily average tropical precipitation accumulation rate (mm day^{-1}) distribution at 1.0° from TMPA with (+0) and without (-0) zero values and the distribution from the GPCP-1DD dataset, both from 1998 to 2008.

Percentiles	TMPA $1^\circ -0$	TMPA $1^\circ +0$	GPCP 1°
10	0.07	0.009	0.07
20	0.247	0.039	0.30
30	0.545	0.102	0.79
40	0.950	0.226	1.69
50	1.545	0.456	3.17
60	2.422	0.873	5.46
70	3.716	1.623	8.87
80	5.690	3.016	13.98
90	9.202	6.000	22.62
95	12.810	9.442	30.84
99	21.789	18.503	48.65

the intensity percentiles for the weather states: fully half of the WS1 systems have precipitation intensities greater than almost all WS3 systems (only about 10% of WS3 systems exhibit intensities $>2 \text{ mm h}^{-1}$). Even WS2 exhibits intensities comparable to WS3. Only about 20% of the suppressed, non-deep-convective events exhibit precipitation intensities $>1 \text{ mm h}^{-1}$. The disparity is less dramatic when the average accumulation rate (mm h^{-1}) is calculated (Fig. 5): the WS1 peak rate is only about twice that of WS3 because the frequency of occurrence of WS3 is much larger than that of WS1 (cf. Lee et al. 2013). Nevertheless, WS12 contributes all of the precipitation when the average daily accumulation rate is $>2 \text{ mm day}^{-1}$ (Table 4).

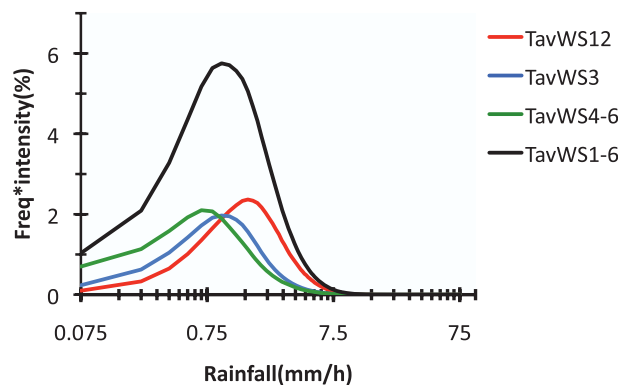


FIG. 4. Distribution of TMPA precipitation intensities (mm h^{-1}) at 3-h intervals averaged to 2.5° and composited for individual ISCCP weather states. For this plot, WS1 and WS2 are combined into WS12 and WS4 through WS6 are combined into WS4–6. The sum of all WS is also shown as WS1–6. The vertical axis shows the frequency of occurrence of each value, binned uniformly at 0.15 mm h^{-1} intervals and multiplied by the intensity to represent the fractional contribution in percent of each intensity range to the total precipitation. The intensities are displayed on a logarithmic scale (which distorts areas) to show the contribution of the largest intensities more clearly.

TABLE 3. Percentile values of the tropical precipitation intensity (mm h^{-1}) distributions from TMPA matched to ISCCP weather states at 3-h, 2.5° intervals. The first column gives the full resolution TMPA distribution percentiles.

Percentiles	$2.5^\circ\text{avg} - 0$	WS1	WS2	WS3	WS4-6
10	0.085	0.639	0.175	0.135	0.044
20	0.221	0.946	0.340	0.287	0.107
30	0.380	1.204	0.490	0.439	0.202
40	0.552	1.447	0.640	0.595	0.320
50	0.738	1.698	0.798	0.761	0.453
60	0.958	1.975	0.98	0.948	0.607
70	1.243	2.316	1.206	1.176	0.792
80	1.646	2.782	1.515	1.484	1.053
90	2.370	3.603	2.050	2.022	1.538
95	3.165	4.469	2.651	2.626	2.097
99	5.312	6.651	4.408	4.369	3.796

To reinforce our interpretation of the differences between the deep convective WS, we composite results from the ISCCP CS and CT products that provide the size and duration distribution of cold cloud objects containing deep convective clouds (remember that cloud system sizes are larger than convective cloud sizes or precipitating cloud sizes). We match each convectively active WS (1, 2, and 3) to the nearest deep convective cloud object and compile size and duration distributions. Given the highly skewed shape of the size distributions, better measures of the size are the distribution percentile values: more than 90% of WS3 systems are smaller than about 75 km, whereas about 70% of WS1 systems are larger than 75 km. The same relative difference in size can be inferred from the frequency of convective clouds in the WS1 and WS3 patterns in Fig. 1. The average duration of the average-sized WS1 (about 125 km radius) is about 6–9 h (cf. Machado et al. 1998), but 90% of all systems with durations >12 h are WS1 systems. Limitations on tracking with the ISCCP dataset exclude most of the WS3 cases, meaning that they have durations <6 h.

What we have shown is that the distribution of precipitation intensity is not determined by precipitation as a single type of phenomenon with a range of values but rather comprises the separate distributions of at least two distinct types of deep convection (with the collection of “non-deep-convective” or shallow convection types contributing most to the smaller intensities). The clear implication is that changes in the distribution of precipitation intensity as part of climate change cannot be considered as a single process—simply a shift of (all) precipitation intensities. The simple alternative between deep convective and non-deep-convective states is usually thought of as a local thermodynamic issue involving the static stability of the atmosphere, but the relationship among the different types of deep convection

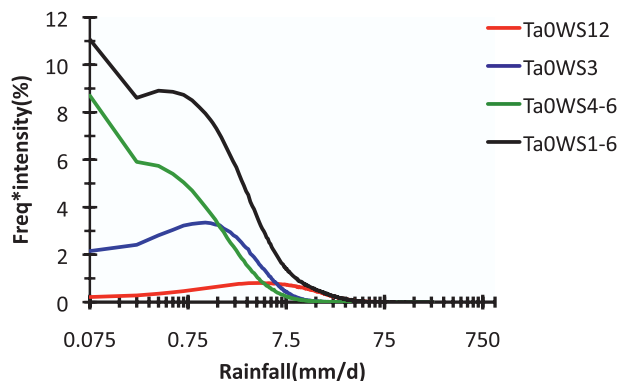


FIG. 5. Distribution of TMPA average daily precipitation accumulation rates (mm day^{-1}) averaged to 2.5° and composited for individual ISCCP weather states. For this plot, WS1 and WS2 are combined into WS12 and WS4 through WS6 are combined into WS4-6. The sum of all WS is also shown as WS1-6. The vertical axis shows the frequency of occurrence of each value, binned uniformly at 0.15 mm day^{-1} intervals and multiplied by the intensity to represent the fractional contribution in percent of each intensity range to the total precipitation. The intensities are displayed on a logarithmic scale (which distorts areas) to show the contribution of the largest intensities more clearly.

is clearly dynamical as suggested by the “switching” behavior documented in MJO events (Tromeur and Rossow 2010) and in the initiation and evolution of African easterly waves (AEWs; Mekonnen and Rossow 2011).

Climate model studies already show that the extreme range of precipitation intensity does not scale like the changes of water vapor abundance, as would be the case if moisture convergence depended only on water vapor abundance (e.g., Emori and Brown 2005; Held and Soden 2006). At the least, the feedback of changing latent heating has to have dynamical consequences. However, all of the climate GCMs currently parameterize tropical deep convection as a single process, localized to individual

TABLE 4. Percentile values for the daily average tropical precipitation accumulation rate (mm day^{-1}) distributions from TMPA matched to ISCCP weather states at 2.5° intervals.

Percentiles	WS1	WS2	WS3	WS456
10	0.148	0.008	0.005	0.001
20	0.317	0.023	0.015	0.004
30	0.491	0.049	0.032	0.008
40	0.676	0.086	0.058	0.015
50	0.879	0.137	0.097	0.026
60	1.115	0.208	0.154	0.045
70	1.414	0.309	0.237	0.078
80	1.827	0.461	0.368	0.138
90	2.544	0.744	0.617	0.279
95	3.292	1.051	0.891	0.468
99	5.227	1.874	1.628	1.100

grid cells (on the order of 25–200 km in size) with short lifetimes (on the order of minutes to a few hours) that most resembles ordinary cumulonimbus (i.e., WS3). As mentioned before, most of these climate models have “extreme” precipitation intensities that are much more characteristic of WS3 (Stephens et al. 2010). In other words, these models do not have anything equivalent to the mesoscale-organized type of deep convection, WS12, and so are not capable of switching from ordinary deep convection to mesoscale-organized deep convection in response to the larger-scale circulation. Wilcox and Donner (2007) show that, in one model at least, introducing a parameterization that tries to represent mesoscale convection makes a much larger difference to the model behavior than global warming does. Since it is the mesoscale deep convective systems that dominate the extreme portion of both the precipitation intensity and accumulation distributions, the changes of precipitation extremes in these models cannot be realistic.

The observed distinctive behavior of the different deep convective storm types undercuts the simple projection of changes of extremes based on the large-scale balances or by a simple scaling. These results draw attention to the need to understand why different deep convective storm types exist, how they interact with each other and with the larger-scale circulation, and what role they each play in the atmospheric general circulation. Until the full range of deep convective processes in the tropics is more realistically represented in climate models, they cannot be used to predict the changes of extreme precipitation events in a changing (warming) climate.

Acknowledgments. The authors acknowledge funding from the NASA MEASURES program administered by Dr. Martha Maiden.

REFERENCES

- Adler, R. F., and Coauthors, 2003: The Version-2 Global Precipitation Climatology Project (GPCP) monthly precipitation analysis (1979–present). *J. Hydrometeorol.*, **4**, 1147–1167.
- Allan, R. P., and B. J. Soden, 2008: Atmospheric warming and the amplification of precipitation extremes. *Science*, **321**, 1481–1484, doi:10.1126/science.1160787.
- Allen, M. R., and W. J. Ingram, 2002: Constraints on future changes in climate and the hydrological cycle. *Nature*, **419**, 224–232, doi:10.1038/nature01092; Corrigendum, **489**, 590.
- Berg, W., T. L’Ecuyer, and J. M. Haynes, 2010: The distribution of rainfall over oceans from spaceborne radars. *J. Appl. Meteor. Climatol.*, **49**, 535–543.
- Cotton, W. R., and R. A. Anthes, 1989: *Storm and Cloud Dynamics*. International Geophysics Series, Vol. 44, Academic Press, 880 pp.
- Emanuel, K. A., 1994: *Atmospheric Convection*. Oxford University Press, 580 pp.
- Emori, S., and S. J. Brown, 2005: Dynamic and thermodynamic changes in mean and extreme precipitation under changed climate. *Geophys. Res. Lett.*, **32**, L17706, doi:10.1029/2005GL023272.
- Feldl, N., and G. H. Roe, 2011: Climate variability and the shape of daily precipitation: A case study of ENSO and the American west. *J. Climate*, **24**, 2483–2499.
- Groisman, P. Ya., R. W. Knight, D. R. Easterling, T. R. Karl, G. C. Hegerl, and V. N. Razuvaev, 2005: Trends in intense precipitation in the climate record. *J. Climate*, **18**, 1326–1350.
- Held, I. M., and B. J. Soden, 2006: Robust responses of the hydrological cycle to global warming. *J. Climate*, **19**, 5686–5699.
- Hourdin, F., and Coauthors, 2006: The LMDZ4 general circulation model: Climate performance and sensitivity to parametrized physics with emphasis on tropical convection. *Climate Dyn.*, **27**, 787–813, doi:10.1007/s00382-006-0158-0.
- Houze, R. A., 2004: Mesoscale convective systems. *Rev. Geophys.*, **42**, RG4003, doi:10.1029/2004RG000150.
- , and P. V. Hobbs, 1982: Organization and structure of precipitating cloud systems. *Advances in Geophysics*, Vol. 24, Academic Press, 225–315.
- Huffman, G. J., R. F. Adler, M. Morrissey, D. T. Bolvin, S. Curtis, R. Joyce, B. McGavock, and J. Susskind, 2001: Global precipitation at one-degree daily resolution from multisatellite observations. *J. Hydrometeorol.*, **2**, 36–50.
- , and Coauthors, 2007: The TRMM multisatellite precipitation analysis (TMPA): Quasi-global, multi-year, combined-sensor precipitation estimates at fine scales. *J. Hydrometeorol.*, **8**, 38–55.
- Jakob, C., and A. P. Siebesma, 2003: A new subcloud model for mass-flux convection schemes: Influence on triggering, updraft properties, and model climate. *Mon. Wea. Rev.*, **131**, 2765–2778.
- , and G. Tselioudis, 2003: Objective identification of cloud regimes in the tropical western Pacific. *Geophys. Res. Lett.*, **30**, 2082, doi:10.1029/2003GL018367.
- , and C. Schumacher, 2008: Precipitation and latent heating characteristics of the major tropical western Pacific cloud regimes. *J. Climate*, **21**, 4348–4364.
- , G. Tselioudis, and T. Hume, 2005: The radiative, cloud and thermodynamic properties of the major tropical western Pacific cloud regimes. *J. Climate*, **18**, 1203–1215.
- Jin, Y., and W. B. Rossow, 1997: Detection of cirrus overlapping low-level clouds. *J. Geophys. Res.*, **102**, 1727–1737.
- Jung, T., and Coauthors, 2010: The ECMWF model climate: Recent progress through improved physical parameterizations. *Quart. J. Roy. Meteor. Soc.*, **136A**, 1145–1160, doi:10.1002/qj.634.
- Katz, R. W., 1999: Extreme value theory for precipitation: Sensitivity analysis for climate change. *Adv. Water Resour.*, **23**, 133–139.
- Kharin, V. V., F. W. Zwiers, X. Zhang, and G. C. Hegerl, 2007: Changes in temperature and precipitation extremes in the IPCC ensemble of global coupled model simulations. *J. Climate*, **20**, 1419–1444.
- Kummerow, C., and Coauthors, 2000: The status of the Tropical Rainfall Measuring Mission (TRMM) after two years in orbit. *J. Appl. Meteor.*, **39**, 1965–1982.
- Lee, D., L. Oreopoulos, G. J. Huffman, W. B. Rossow, and I.-S. Kang, 2013: The precipitation characteristics of ISCCP tropical weather states. *J. Climate*, **26**, 772–788.
- Lenderink, G., and E. van Meijgaard, 2008: Increase in hourly precipitation extremes beyond expectations from temperature changes. *Nat. Geosci.*, **1**, 511–514.

- Lin, B., and W. B. Rossow, 1997: Precipitation water path and rainfall rate estimates for oceans using Special Sensor Microwave Imager and International Satellite Cloud Climatology Project data. *J. Geophys. Res.*, **102** (D8), 9359–9374.
- Luo, Z., G. Y. Liu, G. L. Stephens, and R. H. Johnson, 2009: Terminal versus transient cumulus congestus: A CloudSat perspective. *Geophys. Res. Lett.*, **36**, L05808, doi:10.1029/2008GL036927.
- Machado, L. A. T., and W. B. Rossow, 1993: Structural characteristics and radiative properties of tropical cloud clusters. *Mon. Wea. Rev.*, **121**, 3234–3260.
- , —, R. L. Guedes, and A. W. Walker, 1998: Life cycle variations of mesoscale convective systems over the Americas. *Mon. Wea. Rev.*, **126**, 1630–1654.
- Meehl, G. A., J. M. Arblaster, and C. Tebaldi, 2005: Understanding future patterns of increased precipitation intensity in climate model simulations. *Geophys. Res. Lett.*, **32**, L18719, doi:10.1029/2005GL023680.
- Mekonnen, A., and W. B. Rossow, 2011: The interaction between deep convection and easterly waves tropical North Africa: A weather state perspective. *J. Climate*, **24**, 4276–4294.
- Mohr, K. I., J. S. Famiglietti, and E. J. Zipser, 1999: The contribution to tropical rainfall with respect to convective system type, size, and intensity estimated from the 85-GHz ice-scattering signature. *J. Appl. Meteor.*, **38**, 596–606.
- Moncrieff, M. W., 1981: A theory of organised steady convection and its transport properties. *Quart. J. Roy. Meteor. Soc.*, **107**, 29–50.
- , 1992: Organized convective systems: Archetypal dynamical models, mass and momentum flux theory, and parametrization. *Quart. J. Roy. Meteor. Soc.*, **118**, 819–850.
- , 2004: Analytic representation of the large-scale organization of tropical convection. *J. Atmos. Sci.*, **61**, 1521–1538.
- Nicholls, N., and W. Murray, 1999: Workshop on indices and indicators for climate extremes: Asheville, NC, USA, 3–6 June 1997, Breakout Group B: Precipitation. *Climatic Change*, **42**, 23–29.
- O’Gorman, P. A., and T. Schneider, 2009: The physical basis for increases in precipitation extremes in simulations of 21st-century climate change. *Proc. Natl. Acad. Sci. USA*, **106**, 14 773–14 777, doi:10.1073/pnas.0907610106.
- Oreopoulos, L., and W. B. Rossow, 2011: The cloud radiative effect of ISCCP weather states. *J. Geophys. Res.*, **116**, D12202, doi:10.1029/2010JD015472.
- Rossow, W. B., and R. A. Schiffer, 1999: Advances in understanding clouds from ISCCP. *Bull. Amer. Meteor. Soc.*, **80**, 2261–2287.
- , and Y. Zhang, 2010: Evaluation of a statistical model of cloud vertical structure using combined *CloudSat* and *CALIPSO* cloud layer profiles. *J. Climate*, **23**, 6641–6653.
- , G. Tselioudis, A. Polak, and C. Jakob, 2005a: Tropical climate described as a distribution of weather states indicated by distinct mesoscale cloud property mixtures. *Geophys. Res. Lett.*, **32**, L21812, doi:10.1029/2005GL024584.
- , Y. Zhang, and J. Wang, 2005b: A statistical model of cloud vertical structure based on reconciling cloud layer amounts inferred from satellites and radiosonde humidity profiles. *J. Climate*, **18**, 3587–3605.
- Stephens, G. L., and Y. Hu, 2010: Are climate-related changes to the character of global-mean precipitation predictable? *Environ. Res. Lett.*, **5**, 025209, doi:10.1088/1748-9326/5/2/025209.
- , and Coauthors, 2010: Dreary state of precipitation in global models. *J. Geophys. Res.*, **115**, D24211, doi:10.1029/2010JD014532.
- Trenberth, K. E., A. Dai, R. M. Rasmussen, and D. B. Parsons, 2003: The changing character of precipitation. *Bull. Amer. Meteor. Soc.*, **84**, 1205–1217.
- Tromeur, E., and W. B. Rossow, 2010: Interaction of tropical deep convection with the large-scale circulation in the MJO. *J. Climate*, **23**, 1837–1853.
- Tselioudis, G., and W. B. Rossow, 2011: Time scales of variability of the tropical atmosphere derived from cloud-defined weather states. *J. Climate*, **24**, 602–608.
- Wentz, F. J., L. Ricciardulli, K. Hilburn, and C. Mears, 2007: How much more rain will global warming bring? *Science*, **317**, 233–235, doi:10.1126/science.1140746.
- Wilcox, E. M., and L. J. Donner, 2007: The frequency of extreme rain events in satellite rain-rate estimates and an atmospheric general circulation model. *J. Climate*, **20**, 53–69.
- Zhang, G. J., and N. A. McFarlane, 1995: Sensitivity of climate simulations to the parameterization of cumulus convection in the Canadian Climate Centre general circulation model. *Atmos.–Ocean*, **33**, 407–446.
- Zipser, E. J., D. J. Cecil, C. Liu, S. W. Nesbitt, and D. P. Yorty, 2006: Where are the most intense thunderstorms on Earth? *Bull. Amer. Meteor. Soc.*, **87**, 1057–1071.

Copyright of Journal of Climate is the property of American Meteorological Society and its content may not be copied or emailed to multiple sites or posted to a listserv without the copyright holder's express written permission. However, users may print, download, or email articles for individual use.